Metrol. Meas. Syst., Vol. 32 (2025), No. 4
DOI: 10.24425/mms.2025.155801

METROLOGY AND MEASUREMENT SYSTEMS
Index 330930, ISSN 0860-8229
www.metrology.wat.edu.pl

PRECISE FREQUENCY STABILITY MEASUREMENT TECHNOLOGY BASED ON GROUP PERIOD SYNCHRONIZATION

Bao-Qiang Du, Zi-Lin Liu, Xiang Wang

Hunan Normal University, School of Information Science and Engineering, Changsha, 410081, China (✉ *dubaoqiang@hunnu.edu.cn*)

Abstract

A precise frequency stability measurement technology is proposed utilizing group periodic phase synchronization of signals with varying frequencies. By quantifying the results of phase comparisons between different frequency signals and analyzing these quantized outcomes, high-precision frequency measurements can be achieved. The phase coincidence points between the two comparison signals serve as the start and stop signals for the counter, where the time interval between identical phase coincidence points represents a complete cycle. Through the detection and analysis of phase coincidence points, the ±1 word counting error is eliminated, thereby enhancing the speed of frequency measurement. Employing Field-Programmable Gate Array (FPGA) technology simplifies the measurement apparatus and reduces development costs. Experimental results demonstrate that this method achieves a frequency stability of 10^{-13} at 1s. Compared to traditional frequency measurement technologies, this approach offers significant advantages in terms of power consumption, equipment size, and measurement rate, making it crucial for high-tech applications such as Beidou satellite positioning, precision timing, high-precision time-frequency transmission and comparison, and scientific metrology.

Keywords: frequency stability, frequency measurement, group period synchronization, group quantization.

1. Introduction

With the development of aeronautics and astronautics, ubiquitous location services and their scale applications, air, land and sea integration, high-tech communication, and high precision radar detection, the measurement precision of frequency signals, especially for the radio frequency signals, is required to be higher [1-3]. At present, usually used frequency detection technologies are mainly pulse frequency measurement technology, multicycle synchronous measurement technology, analog interpolation detection technology and time vernier measurement technology, *etc.* The pulse frequency measurement and multicycle synchronous measurement technologies exist the counting error with ±1 word [4-6]. Due to the filling frequencies often no more than 10^{-9} Hz, the precision of the frequency detection is often no more than 10^{-9} Hz. The produced frequency detection meter via these methods has the characteristics of simple equipment structure and low development cost, but its detection precision is relatively low. The multicycle synchronous frequency measurement technology [7, 8] is developed based on pulse frequency measurement technology and has widespread applications in current frequency measurement systems. In this frequency measurement method, the actual gate is not a fixed value, but an integer multiple of the measured signal period, *i.e.* synchronized with the measured signal, thus eliminating the ±1 word counting error when counting the measured signal. The measurement precision has been greatly improved and equal precision measurement has been achieved throughout the measurement frequency range. In the entire measurement frequency range, multicycle synchronous frequency measurement technology has made obvious progress over pulse frequency measurement technology, but it

Article history: received March 4, 2025; revised May 21, 2025; accepted July 3, 2025; available online September 19, 2025.

also has its disadvantages: it cannot perform continuous frequency measurement, and in the case of fast measurement requirements, due to the need for high measurement precision, a higher frequency standard must be used, which requires a larger number of bits in the frequency standard counter (usually 24 bits or 32 bits). This not only consumes a large amount of hardware resources but also requires more instruction cycles and loops when processing data with 8-bit or 16-bit single chip microcomputers, especially for multiplication and division operations. The analog interpolation detection technology [9, 10] is a measurement method that relies on the measured time interval, primarily addressing the challenge of quantizing decimal units. This technology comprises two main components: coarse and fine measurements. Coarse measurement involves determining the integer portion of the time interval using a pulse counting method, while fine measurement focuses on capturing the fractional part through interpolation. In fine measurement, the "boot" interpolation device (interpolation time extender) amplifies the fractional component by a factor of 1000. Specifically, a constant current source charges a capacitor at fractional time intervals and discharges it back to its original voltage level within 999 fractional times of the charging duration. The control gate of the interpolation time extender opens upon receiving the start pulse and closes when the capacitor returns to its initial voltage level. The primary advantage of interpolation is its high theoretical measurement precision, increasing resolution by three orders of magnitude. However, a ±1 word count error persists. Additionally, due to the nonlinearity of capacitor charge and discharge, this nonlinearity increases over time, limiting the expansion coefficient and making it difficult to achieve higher precision in practical circuit implementations. While this technology does not require a high clock frequency, the analog circuitry can be affected by distributed parameters and noise interference, especially when measuring signals near microwave frequencies. Consequently, in continuous high-frequency measurements, the circuit's response speed also constrains measurement precision. Currently, the HP5360A oscilloscope exemplifies time interval counter products utilizing anti-number interpolation principles. This counter features a charging time that is only one thousandth of the capacitor discharge time, achieving a measurement resolution of 0.1 ns, which meets the precision requirements for many scientific experiments and engineering applications. Although the ±1 word count error remains in analog interpolation detection and time vernier measurement technologies [11, 12], it can be reduced to approximately 0.0001 using an interpolator, with detection precision reaching 10^{-11}. Frequency detection instruments employing these methods offer good precision but have complex system structures and designs, leading to high development costs that limit their widespread application [13-15]. Phase coincidence detection technology [16-18] effectively eliminates the ±1 word count error in frequency detection, achieving a frequency detection precision of 10^{-10}. However, the phase coincidence point is non-unique and random, hindering further improvements in frequency detection precision.

Therefore, n precise frequency stability measurement technology based on group periodic synchronization has been proposed. By integrating the change rule of the group period with the frequency relationship of the compared signal, this technology addresses several issues in phase coincidence detection, simplifies equipment, reduces development costs, and enhances system frequency measurement precision.

2. Measurement principle

Extensive experimental evidence demonstrates that the phase coincidence points of two signals with distinct frequencies recur at intervals corresponding to the group period, adhering to the group period synchronization principle [19, 20]. This phenomenon can be leveraged for precise frequency measurement through the application of variation methods [21].

Consider two stable signals, f_A and f_B, with periods T_A and T_B, respectively. The relationship between these two signals is as follows:

$$T_A = BT_{max\,c}, \tag{1}$$

$$T_B = AT_{max\,c}, \tag{2}$$

$$T_{min\,c} = ABT_{max\,c}. \tag{3}$$

In (3), *A* and *B* (*A* > *B*) are integers greater than zero, respectively. The $T_{max\,c}$ is the greatest common divisor between T_A and T_B, called the greatest common factor period and is the most basic unit in which the phase difference is quantized, also known as the quantization phase shift resolution or measurement resolution, and the $T_{min\,c}$ is called the least common multiple period. As shown in Fig. 1. The f_{out} is the result of different frequency phase comparison or the phase difference between two different frequency signals.

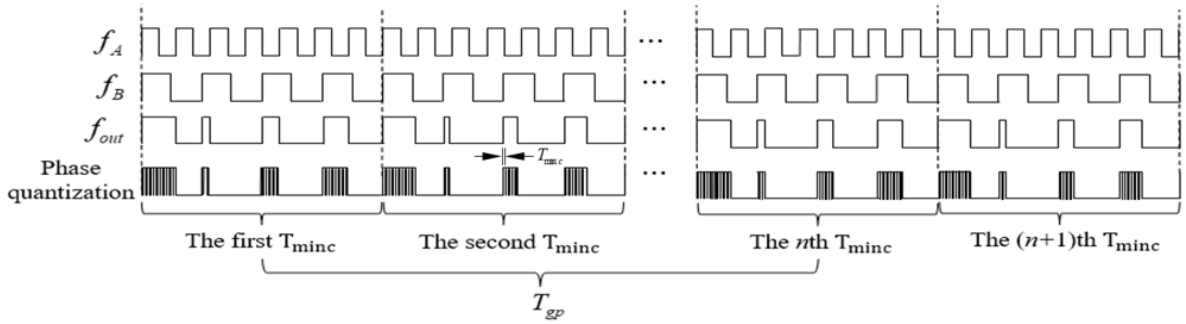

Fig. 1. Group period phase synchronization. f_A and f_B *A* and *B* are two distinct frequency phase comparison signals, f_{out} is the result of the distinct phase comparison between signals f_A and f_B, $T_{min\,c}$ is the least common multiple period between signals f_A and f_B, and T_{gp} is group period between signals f_A and f_B.

As illustrated in Fig. 1, the traditional phase comparison method cannot utilize the period of a specific frequency signal as a reference time for phase processing between different frequency signals for direct phase comparison. This limitation is the primary reason why traditional phase processing methods require frequency normalization and must be conducted under conditions of identical frequencies. Specifically, within the least common multiple period, f_A serves as the measured signal while f_B acts as the reference signal. For each rising edge of signal f_B, the time difference between the rising edge of f_B and the nearest rising edge of the measured signal f_A is defined as the direct time difference between signals f_A and f_B. The phase comparison result is then quantized by filling the phase comparison results with a high-frequency clock.

As you can see, in a $T_{min\,c}$,

$$T_{min\,c} = AT_A = BT_B. \tag{4}$$

When the f_A and f_B keep integer multiples, the phase differences in a $T_{min\,c}$ are shown in (5).

$$\begin{bmatrix}\Delta h_1\\ \Delta h_2\\ \vdots\\ \Delta h_B\end{bmatrix} = \begin{bmatrix}n_1T_A - 1T_B\\ n_2T_A - 2T_B\\ \vdots\\ AT_A - BT_B\end{bmatrix} = \begin{bmatrix}n_1BT_{\max c} - 1AT_{\max c}\\ n_2BT_{\max c} - 2AT_{\max c}\\ n_2BT_{\max c} - 3AT_{\max c}\\ \vdots\\ ABT_{\max c} - BAT_{\max c}\end{bmatrix} = \begin{bmatrix}n_1B - 1A\\ n_2B - 2A\\ n_2B - 3A\\ \vdots\\ AB - BA\end{bmatrix} T_{\max c} = \begin{bmatrix}K_1\\ K_2\\ K_3\\ \vdots\\ K_B\end{bmatrix} T_{\max c}. \tag{5}$$

From the (5), the Δh_1, Δh_2, ... , and Δh_B are some phase differences in the $T_{\min c}$, that is, phase difference values in the f_{out} and n_1, n_2, n_3,⋯, *A* are the T_A numbers f_A for f_B front edge pulses.

The $(K_1, K_2, K_3, \cdots, K_B)^T$ are some positive integers. In fact, K_B is equal to zero, which means that the two comparison signals f_A and f_B coincide completely.

When the signals f_A and f_B do not keep integer multiples, let $T_B^{'} = T_B - \Delta t$, Δt is the phase drift caused by the frequency deviation Δf between the signals f_A and f_B. As shown in Fig. 2.

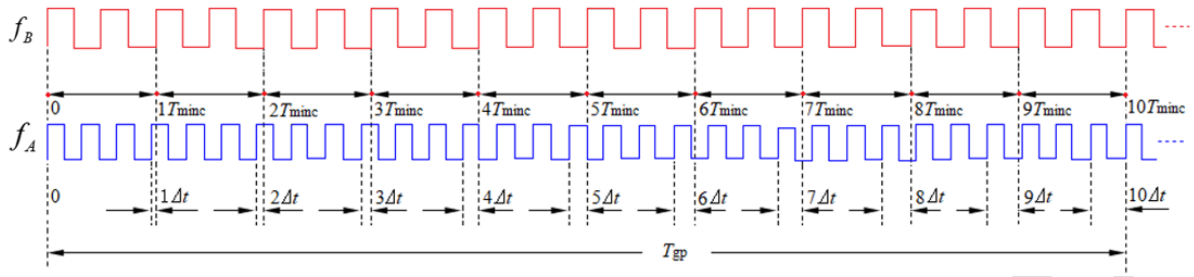

Fig. 2. Generation of phase drift.

The phase differences in a $T_{\min c}$ are described below. The differences of phases within the 1-st $T_{\min c}$ are

$$\begin{bmatrix} \Delta h_{11} \\ \Delta h_{12} \\ \vdots \\ \Delta h_{1B} \end{bmatrix} = \begin{bmatrix} n_1 - T_B' \\ n_2 T_A - 2T_B' \\ \vdots \\ AT_A - BT_B' \end{bmatrix} = \begin{bmatrix} n_1 T_A - T_B + \Delta t \\ n_2 T_A - 2T_B + 2\Delta t \\ \vdots \\ B\Delta t \end{bmatrix}. \tag{6}$$

The differences of phases within the 2nd $T_{\min c}$ are

$$\begin{bmatrix} \Delta h_{21} \\ \Delta h_{22} \\ \vdots \\ \Delta h_{2B} \end{bmatrix} = \begin{bmatrix} (A+n_1)T_A - (B+1)T_B' \\ (A+n_2)T_A - (B+2)T_B' \\ \vdots \\ (A+A)T_A - (B+B)T_B' \end{bmatrix} = \begin{bmatrix} (A+n_1)T_A - (B+1)(T_B - \Delta t) \\ (A+n_2)T_A - (B+2)(T_B - \Delta t) \\ \vdots \\ (A+A)T_A - (B+B)(T_B - \Delta t) \end{bmatrix} = \begin{bmatrix} n_1 T_A - T_B + B\Delta t + \Delta t \\ n_2 T_A - 2T_B + B\Delta t + 2\Delta t \\ \vdots \\ 2B\Delta t \end{bmatrix}. \tag{7}$$

The differences of phases within the 3rd $T_{\min c}$ are

$$\begin{bmatrix} \Delta h_{31} \\ \Delta h_{32} \\ \vdots \\ \Delta h_{3B} \end{bmatrix} = \begin{bmatrix} (2A+n_1)T_A - (2B+1)T_B' \\ (2A+n_2)T_A - (2B+2)T_B' \\ \vdots \\ (2A+A)T_A - (2B+B)T_B' \end{bmatrix} = \begin{bmatrix} (2A+n_1)T_A - (2B+1)(T_B - \Delta t) \\ (2A+n_2)T_A - (2B+2)(T_B - \Delta t) \\ \vdots \\ (2A+A)T_A - (2B+B)(T_B - \Delta t) \end{bmatrix} = \begin{bmatrix} n_1 T_A - T_B + 2B\Delta t + \Delta t \\ n_2 T_A - 2T_B + 2B\Delta t + 2\Delta t \\ \vdots \\ 3B\Delta t \end{bmatrix}. \tag{8}$$

The differences of phases within the $(n-1)$-th $T_{\min c}$ are

$$\begin{bmatrix}\Delta h_{(n-1)1}\\ \Delta h_{(n-1)2}\\ \vdots\\ \Delta h_{(n-1)B}\end{bmatrix}=\begin{bmatrix}[(n-1)A+n_1]T_A-[(n-1)B+1]T_B'\\ [(n-1)A+n_2]T_A-[(n-1)B+2]T_B'\\ \vdots\\ [(n-1)A+A]T_A-[(n-1)B+B]T_B'\end{bmatrix}=$$
$$\begin{bmatrix}[(n-1)A+n_1]T_A-[(n-1)B+1](T_B-\Delta t)\\ [(n-1)A+n_2]T_A-[(n-1)B+2](T_B-\Delta t)\\ \vdots\\ [(n-1)A+A]T_A-[(n-1)B+B](T_B-\Delta t)\end{bmatrix}= \tag{9}$$
$$\begin{bmatrix}n_1T_A-T_B+(n-1)B\Delta t+\Delta t\\ n_2T_A-2T_B+(n-1)B\Delta t+2\Delta t\\ \vdots\\ (n-1)B\Delta t\end{bmatrix}.$$

The differences of phases within the n-th $T_{\min c}$ are

$$\begin{bmatrix}\Delta h_{n1}\\ \Delta h_{n2}\\ \vdots\\ \Delta h_{nB}\end{bmatrix}=\begin{bmatrix}(nA+n_1)T_A-(nB+1)T_B'\\ (nA+n_2)T_A-(nB+2)T_B'\\ \vdots\\ (nA+A)T_A-(nB+B)T_B'\end{bmatrix}=$$
$$\begin{bmatrix}(nA+n_1)T_A-(nB+1)(T_B-\Delta t)\\ (nA+n_2)T_A-(nB+2)(T_B-\Delta t)\\ \vdots\\ (nA+A)T_A-(nB+B)(T_B-\Delta t)\end{bmatrix}=\begin{bmatrix}n_1T_A-T_B+nB\Delta t+\Delta t\\ n_2T_A-2T_B+nB\Delta t+2\Delta t\\ \vdots\\ nB\Delta t\end{bmatrix}. \tag{10}$$

From (6) to (10), it is evident that during the phase comparison of different frequencies, a discernible pattern emerges in the changes of phase differences. Specifically, for adjacent $T_{\min c}$ values, the phase difference corresponds to $B\Delta t$, expressed as $\Delta h_{nB}-\Delta h_{(n-1)B}=B\Delta t$. At the same position, the phase difference between the first and the nth $T_{min\,c}$ is also equal to this value. When $nB\Delta t$ equals T_B, the timing of phase coincidence points exhibits periodic variation. The time interval between these periodic changes is defined as the group period T_{gp}, denoted as

$$T_{gp}=nB\Delta t+nT_{\min c}. \tag{11}$$

Consequently, the T_{gp} can be determined by observing the time interval between the periodic changes of the f_{out}, and the Δt can be calculated by the $nB\Delta t=T_B$

$$\Delta t=\frac{T_B}{nB}=\frac{T_BT_{min\,c}}{nT_{min\,c}B}\approx\frac{T_BT_{min\,c}}{T_{gp}B} \tag{12}$$

Thus, the signal T_B' can be calculated by the formula $T_B'=T_B+\Delta t$.

$$T_B'=T_B+\Delta t=T_B+\frac{T_BT_{min\,c}}{T_{gp}B}. \tag{13}$$

From (12), it is evident that the actual measurement error is significant. A word count error of ±1 at a count of f_{out} results in the actual measurement being an integer multiple of the T_{gp}. Although the period is small, such an error is unacceptable. Through the analysis of $T_{\min c}$ and T_{gp}, we have derived the variation law of phase difference. When two identical phase differences occur simultaneously, it constitutes a group period, as illustrated in Fig. 1. T_A and

T_B' are counted within a group period, yielding N_1 and N_2 respectively, leading to formula (14). The left and right sides of (14) represent integer multiples of the group period.

$$N_1 T_A = N_2 T_B^{'} \tag{14}$$

As shown in Fig. 1, the third phase coincidence point of the first $T_{min\,c}$ coincides with the third phase coincidence point of the n-th $T_{min\,c}$, and this repetition occurs simultaneously with T_{gp}. The count of the third coincidence point at the first time point serves as the opening signal for the gate, while the count of the third coincidence point at the nth time point serves as the closing signal for the gate. By calculating f_A and f_B between the on and off signals respectively, the frequency of f_A can be determined using (14).

Based on the change law of the group period, a precise frequency link between different frequency signals is established, allowing the detection of the measured signal's period using a reference signal. Due to the inherent regularity between the two signals, the same phase coincidence point repeats. If the f_{out} signals between f_A and f_B are processed, and then the phase quantization result of the phase coincidence point is detected by a high-frequency clock, the phase coincidence information can be easily obtained. Simultaneously counting f_A, f_B, and phase coincidence points, using the phase coincidence points to generate a grid, and then counting f_A and f_B at the same grid time can overcome the measurement error caused by the counting error.

If the count of the phase coincidence point has a counting error of ±1 word, with a probability of 50%, the closing signal will inevitably appear within an integer multiple of the group period. Therefore, multiplying both sides of (14) by an integer coefficient $k$can mitigate the impact of the counting error.

$$kN_1 T_A = kN_2 T_B^{'} \tag{15}$$

Consequently, in frequency measurement, even if the counting error of the phase coincidence point is ±1 word, it does not affect the frequency measurement result. However, such a counting error would prolong the gate time and slow down the measurement speed.

3. Measurement scheme

According to the principle of frequency detection based on phase coincidence points, enhancing the precision of frequency detection hinges on precisely acquiring and measuring these phase coincidence points. After reshaping, the signals f_A and f_B undergo phase comparison, yielding f_{out} phase coincidence points. Subsequently, the leading and trailing edges of these phase coincidence points are extracted, and high-frequency clock counts are conducted between these edges. The identical counting results serve as trigger signals for turning on and off, which are then transmitted to the *micro controller unit* (MCU) for data processing and execution. Fig. 3 illustrates the design scheme for frequency detection in this system.

The TSG4102A RF signal generator is utilized to produce the test signal, specifically a sine wave with an amplitude of 3.3 V. The reference signal is supplied by the BVA8607B-M high-stability crystal oscillator. Both the measurement and reference signals are connected to the FPGA via its global clock pin. In this experiment, a 100 MHz and a 1 GHz signal are generated through an internal *phase-locked loop* (PLL) within the FPGA. The 100 MHz signal serves as a delay mechanism for both the reference and measured signals to generate narrow pulse signals. Initially, these narrow pulses are transmitted to a phase comparison module at different frequencies to create a set of cycle compositions. Subsequently, the output f_{out} is quantified and counted using the high-frequency clock generated by the FPGA's internal PLL. The time of the phase coincidence point is selected as the start signal for the counter, which begins

counting the pulses of signals f_A and f_B. The same phase coincidence point acts as the stop signal for the counter, completing the pulse count of both the reference and measurement signals within the gate time. Finally, the pulse counts of the reference and measured signals are transmitted to the data processing module via a serial port instantiated by the FPGA. The data processing module calculates the frequency measurement result of the measured signal using (14).

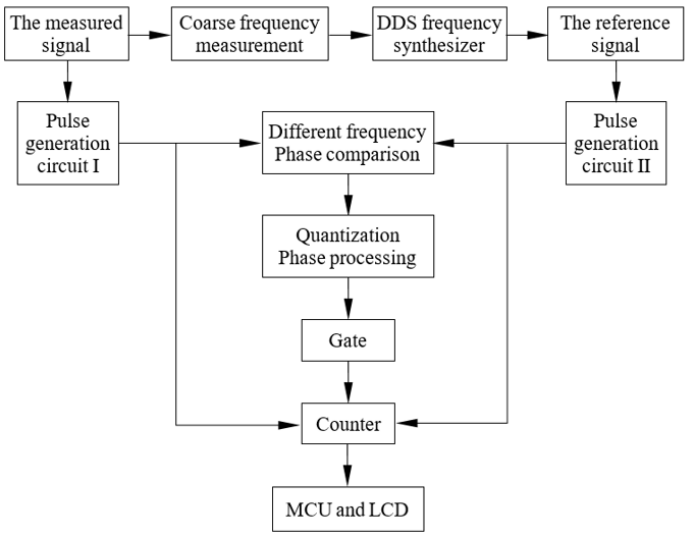

Fig. 3. Frequency detection design scheme on group period synchronization.

3.1. Narrow Pulse Extraction

Since the FPGA can directly recognize sinusoidal waves within the chip and convert them into square wave pulse signals, the two phase comparison signals can be directly transmitted to the FPGA's clock pin without requiring a signal shaping circuit, as illustrated in Fig. 4.

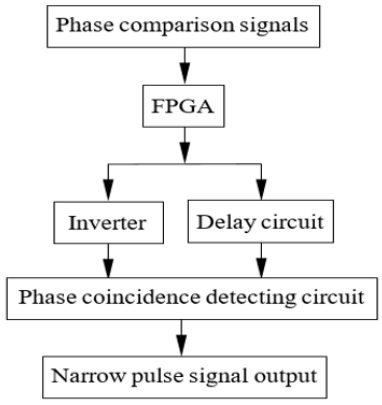

Fig. 4. Narrow apulse extraction scheme.

In Fig. 4, the delay circuit is composed of D flip-flops within the FPGA. By adjusting the clock period of the D flip-flop, the pulse width becomes more suitable for the required delay. Besides providing inherent delay, this circuit also reduces noise in the comparison signal. The square wave pulse signal is sent to an inverter, generating another signal with a phase opposite to the original square wave pulse. These inverse and delayed square wave pulse signals are then transmitted to a phase coincidence detection circuit composed of "AND" logic gates, resulting in narrow pulse signals with the same frequency as the square wave pulses. Converting the

comparison signals into narrow pulses of the same frequency facilitates the formation of phase co-incidence points, synchronizes the phase coincidence fuzzy region with the group period interval, and enhances the stability of the gate, thereby improving the precision of frequency detection, as shown in Fig. 5.

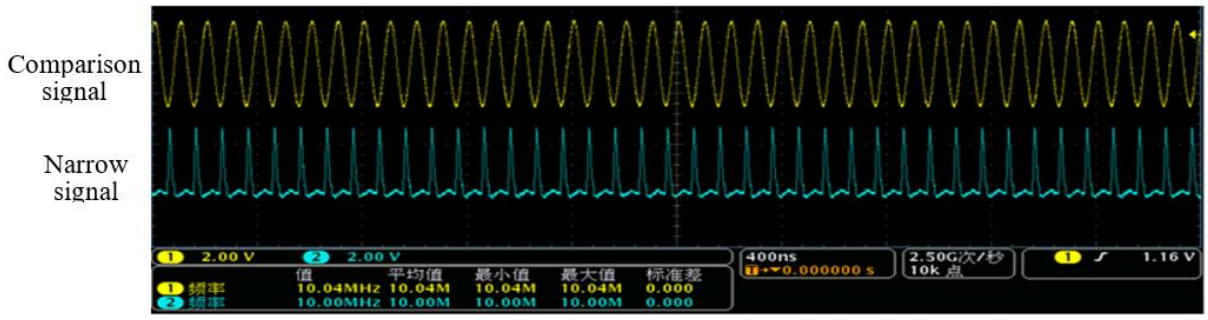

Fig. 5. Narrow pulse extraction results.

3.2. Different Frequency Phase Comparison

Figure 6 is the different frequency phase comparison scheme.

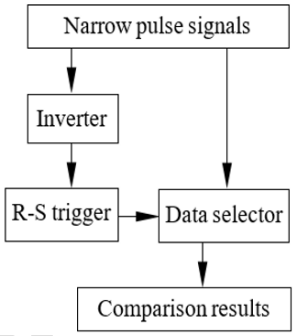

Fig. 6. Different frequency phase comparison scheme.

Following the extraction of pulse signals, both the measured and reference signals are simultaneously converted into narrow pulses of identical frequency. This conversion facilitates phase difference processing by reducing uncertainties associated with the prolonged rise time of sine wave signals, thereby enhancing the stability of phase comparisons. The phase comparison results can be obtained by inputting the narrow pulses, which have the same frequency as the reference and measured signals, into a phase comparison processing module designed for different frequencies. The process for generating these phase comparison results is as follows: the reference signal f_B and the measured signal f_A are fed into the R and S terminals of an R-S flip-flop, respectively. When f_B and f_A exhibit differing levels specifically when $f_B \to 0$, $f_A \to 1$ or $f_B \to 1$, $f_A \to 0$, the R-S flip-flop out-puts a high-level "1" signal. If both f_B and f_A are at a low level "0", the output remains in a hold state. Conversely, when both signals are at a high level "1", indicating either zero phase difference or complete overlap between the reference and measured pulse signals, the R-S flip-flop outputs a low-level "0" signal. As illustrated in Fig. 7, theoretical analysis aligns well with experimental outcomes. In Fig. 7, the f_A represents the measured signal, the f_B represents the reference signal, and the f_{out} represents the different frequency phase comparison results.

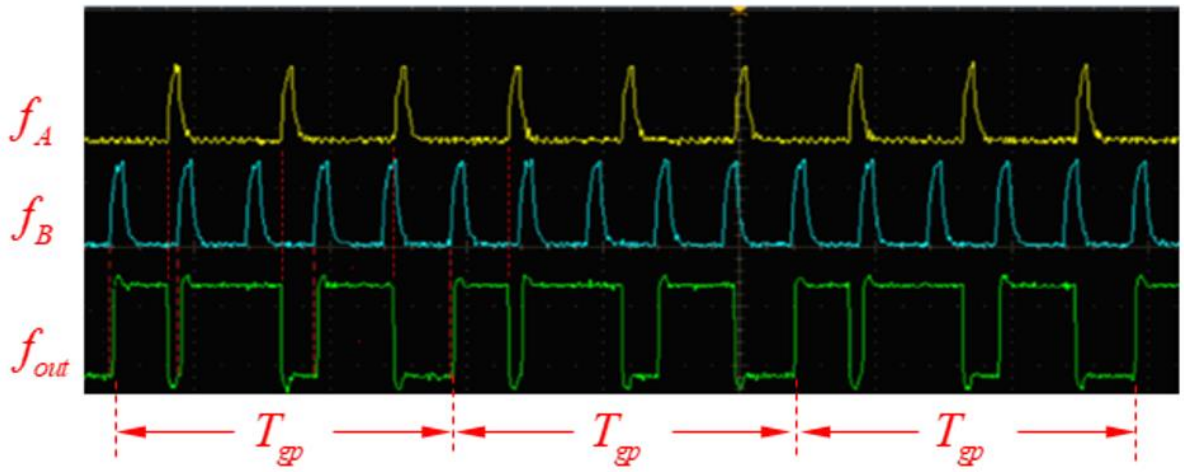

Fig. 7. Different frequency phase comparison results.

3.3. Different Frequency Phase Quantization

Subsequently, following the extraction of the f_{out} frequency in Fig. 7, the phase comparison results undergo quantization using a high-frequency clock within the FPGA chip. This process facilitates more convenient handling of the f_{out} frequency and selection of gate signals, as depicted in Fig. 8.

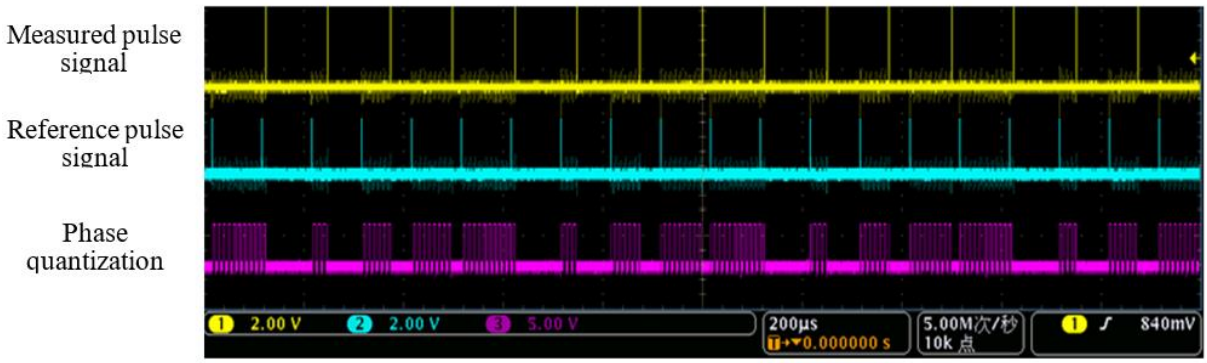

Fig. 8. Quantizing phase processing results.

As shown in Fig. 8, each phase coincidence point is quantified during the phase comparison process. PLL from FPGA provide high-frequency quantized clocks. The quantized phase coincidence points are counted by a high-frequency quantization clock. The moment when two count results match marks the counting gate. Quantizing phase coincidence points aids in processing phase coincidence fuzzy bands. By calculating the width of the coincidence point, the peak value within the fuzzy region can be detected. The timing of the peak appearance within the fuzzy area serves as the switching time for the counting gate, enabling seamless counting. Consequently, changes in the gapless value reflect the stability in frequency measurement.

4. Experiment and its analysis

We have developed a high-precision group periodic synchronization frequency detection system. This system has a measurement range of 1-20 MHz and achieves a second-level frequency stability of 10^{-13}. In the frequency detection experiment, a cesium atomic clock

5071A providing a 10 MHz external reference clock was utilized to verify the measurement precision of the system. A TSG4102A RF signal generator with a second-level frequency stability of 2×10^{-11} generated the measured signals. Operation of the system is straightforward: first, connect the RF output of the signal generator to the signal input of the frequency detection system. Next, adjust the signal generator to produce test signals such as 16.384 MHz and 10.354 MHz, and output them to the input end of the frequency detection system. Then, press the "Measure" button on the frequency detection system, and the frequency measurement results, frequency stability, and frequency differences will be displayed on the LCD screen. Table 1 presents the experimental results of the system's frequency measurements.

The second-level stability of frequency measurement of the system, as indicated in Table 1, reaches 10^{-13}. Since the two comparison signals originate from different frequency sources, their phase noise cumulatively affects the system's measurement error, leading to jitter in the phase comparison results. Within the gate time, the counting of the two comparison signals introduces errors, which are then processed by a microcontroller to reduce the system's frequency stability. Although phase comparison results are not directly used for frequency detection, this approach suppresses measurement errors to some extent. In practical applications, increasing the FPGA system's clock frequency and optimizing the upper computer algorithm can improve frequency stability, thereby minimizing additional noise influence and achieving measurement results with frequency stability better than 10^{-13} s^{-1} or even higher. Additionally, the stability of the frequency relationship between the reference signal and the measured signal is also an important factor, as this directly affects the generation of group period and phase quantization. It will cause the jitter of the measurement gate and reduce the precision of the frequency measurement.

Table 1. Frequency measurement experiment results.

The measured frequency [MHz]	Measurement results [Hz]	Frequency differences [Hz]	Frequency stability (1s)
6.4960	6495999.455	0.544	5.26×10^{-13}
10.354	10353999.188	0.811	2.35×10^{-13}
11.340	11339997.628	2.371	6.69×10^{-13}
11.917	11916997.238	2.761	5.21×10^{-13}
12.071	12070997.004	2.995	3.91×10^{-13}
12.880	12879996.967	3.023	2.91×10^{-13}
12.685	12684996.867	3.132	2.86×10^{-13}
13.560	13559996.549	3.450	6.39×10^{-13}
15.615	15614996.211	3.788	2.21×10^{-13}
15.754	15753996.236	3.763	2.97×10^{-13}
16.384	16383999.849	0.150	1.76×10^{-13}
18.023	18022996.541	3.458	7.09×10^{-13}

Compared to traditional frequency measurement methods, the frequencies listed in Table 1 were measured using three different instruments: the HP5360A time interval counter based on the traditional analog interpolation method, the HP5390A frequency stability analyzer utilizing the traditional beat method, and the 5110A frequency stability analyzer employing the double mixing time difference method. The experimental results indicate that the frequency measurement precision is less than 10^{-13}, with a frequency deviation exceeding 4 Hz. Additionally, the K+K FXE phase frequency counter, a comprehensive commercial universal frequency counter currently available on the market, achieves a frequency measurement

precision of 4×10^{-13} and has been widely adopted in the field of time-frequency analysis. The precision index of the proposed meth-od is comparable to that of the K+K FXE frequency counter. Therefore, compared to traditional frequency detection methods, which are characterized by complex structures, large sizes, high equipment costs, and relatively low comparison precision, the frequency measurement scheme presented in this paper offers a simpler structure, ease of integration, lower equipment costs, higher comparison precision, a wider application range, and broader prospects. This method primarily focuses on short-term stability or frequency measurement between precision frequency source signals, rather than long-term frequency stability of frequency sources as a primary metric within its application scope.

5. Conclusion

The precision frequency stability measurement technology based on group period synchronization introduced in this paper does not rely on improvements in circuitry or advancements in microelectronic devices to enhance measurement precision through conventional frequency measurement technology. Instead, it leverages the inherent interrelationships and change laws between frequency signals. These principles are applied to the interoperable processing of periodic signals, enabling phase detection and processing of non-normalized frequencies. According to the distribution law of phase between different frequency signals, phase measurement is utilized for gate selection, thereby overcoming challenges associated with finding phase comparison results and addressing randomness issues. Experimental results demonstrate that the proposed method can achieve a second-level frequency stability of 10^{-13}. Compared to traditional frequency measurement technology such as time cursor, phase comparison, and analogy interpolation [22-24], this technology exhibits high measurement precision, a simple system structure, low development costs, and high system stability. With advancements in modern electronic science and improvements in FPGA integration technology, the measurement precision of this new frequency measurement system may be further enhanced, leading to more extensive applications in the field of precision time-frequency measurement.

Acknowledgements

This work was funded by the National Natural Science Foundation of China (No. 62173140), Key Research and Development Project of Hunan Province (No. 2022GK2067), and Natural Science Foundation of Hunan Province (No. 2025JJ50408).

References

[1] Wang, D., Zhang, X., An, X., Ding, Y., Li, J., & Dong, W. (2023). Microwave frequency measurement system using fixed low frequency detection based on photonic assisted brillouin technique. *IEEE Transactions on Instrumentation and Measurement*, *72*, 1–10. https://doi.org/10.1109/tim.2023.3256465

[2] Li, S., Qing, T., Fu, J., Wang, X., & Pan, S. (2020). High-Accuracy and fast measurement of optical transfer delay. *IEEE Transactions on Instrumentation and Measurement*, *70*, 1–4. https://doi.org/10.1109/tim.2020.3011585

[3] Zhang, X., Cheng, P., Ci, Y., & Tian, S. (2015). Microwave frequency measurement method using microwave phase detection. *IET Science Measurement & Technology*, *10*(3), 234–238. https://doi.org/10.1049/iet-smt.2015.0086

[4] Ge, J., Wang, M., Hu, X., Xu, W., Luo, W., Feng, K., Zhang, Y., Wang, K., Wang, G., Dong, H., & Liu, Z. (2024). High-precision frequency measurement approach of diminishing multi-source errors for UAV-based aeromagnetic survey. *Measurement*, *227*, 114312. https://doi.org/10.1016/j.measurement.2024.114312

[5] Du, B., & Tan, L. (2024). High-Accuracy phase frequency detection technology based on BDS time and frequency signals. *Sensors*, *24*(14), 4606. https://doi.org/10.3390/s24144606

[6] Zhu, B., Xue, M., Yu, C., & Pan, S. (2021). Broadband instantaneous multi-frequency measurement based on chirped pulse compression. *Chinese Optics Letters*, *19*(10), 101202. https://doi.org/10.3788/col202119.101202

[7] Xia, S., Xiao, Y., Chen, B., & Zhang, H. (2025). A novel method for microwave frequency measurement based on frequency-to-time mapping. *IEEE Transactions on Instrumentation and Measurement*, 1. https://doi.org/10.1109/tim.2025.3551566

[8] Zhou, P., Tang, Z., Zhu, J., & Li, N. (2023). Instantaneous frequency measurement using Photonics-Assisted broadband signal generation and processing. *IEEE Microwave and Wireless Technology Letters*, *33*(5), 619–622. https://doi.org/10.1109/lmwt.2023.3235361

[9] McEwan, A., & Collins, S. (2006). Direct Digital-Frequency Synthesis by analog interpolation. *IEEE Transactions on Circuits and Systems II Analog and Digital Signal Processing*, *53*(11), 1294–1298. https://doi.org/10.1109/tcsii.2006.882349

[10] Gammoh, K., Peterson, C. K., Penry, D. A., & Wood, S. C. (2020). Linearity Theory of Stochastic Phase-Interpolation Time-to-Digital Converter. *IEEE Transactions on Circuits and Systems I Regular Papers*, *67*(12), 4348–4359. https://doi.org/10.1109/tcsi.2020.3013709

[11] Cui, K., & Li, X. (2019). A High-Linearity Vernier Time-to-Digital converter on FPGAs with improved resolution using Bidirectional-Operating Vernier delay lines. *IEEE Transactions on Instrumentation and Measurement*, *69*(8), 5941–5949. https://doi.org/10.1109/tim.2019.2959423

[12] Andersson, N. U., & Vesterbacka, M. (2014). A Vernier Time-to-Digital Converter with delay latch chain architecture. *IEEE Transactions on Circuits & Systems II Express Briefs*, *61*(10), 773–777. https://doi.org/10.1109/tcsii.2014.2345289

[13] Liu, J., Shi, T., & Chen, Y. (2020). High-Accuracy multiple microwave frequency measurement with Two-Step accuracy improvement based on stimulated brillouin scattering and Frequency-to-Time mapping. *Journal of Lightwave Technology*, *39*(7), 2023–2032. https://doi.org/10.1109/jlt.2020.3044251

[14] Xue, M., Lv, M., Wang, Q., Zhu, B., Yu, C., & Pan, S. (2021). Broadband optoelectronic frequency response measurement utilizing frequency conversion. *IEEE Transactions on Instrumentation and Measurement*, *70*, 1–5. https://doi.org/10.1109/tim.2021.3079562

[15] Wang, D., Zhang, X., Zhao, X., Yang, Z., & Dong, W. (2022). Photonic microwave frequency measurement with improved resolution based on bandwidth-reduced stimulated Brillouin scattering. *Optical Fiber Technology*, *68*, 102803. https://doi.org/10.1016/j.yofte.2021.102803

[16] Du, N. B., Dong, N. S., Wang, N. Y., Guo, N. S., Cao, N. L., Zhou, N. W., Zuo, N. Y., & Liu, D. (2013). High-resolution frequency measurement method with a wide-frequency range based on a quantized phase step law. *IEEE Transactions on Ultrasonics Ferroelectrics and Frequency Control*, *60*(11), 2237–2243. https://doi.org/10.1109/tuffc.2013.6644729

[17] Huang, C., & Chan, E. H. W. (2021). All-Optical Pulsed Signal Doppler Frequency Shift Measurement System. *IEEE Photonics Journal*, *13*(6), 1–7. https://doi.org/10.1109/jphot.2021.3118679

[18] Lukin, K. A., Vyplavin, P. L., Palamarchuk, V. P., Kudriashov, V. V., Kulpa, K., Gajo, Z. K., Misiurewicz, J., & Kulpa, J. S. (2015). Phase measurement accuracy in noise waveform synthetic aperture radar. *IEEE Transactions on Aerospace and Electronic Systems*, *51*(4), 3364–3373. https://doi.org/10.1109/taes.2015.140537

[19] Du, B., Shi, L., Chen, Y., Dong, S., Yang, Z., Cao, L., & Guo, S. (2014). Phase group synchronization between any signals and its physical characteristics. *Science China Physics Mechanics and Astronomy*, *57*(4), 674–679. https://doi.org/10.1007/s11433-013-5194-2

[20] Burt, E. A., Yi, L., Tucker, B., Hamell, R., & Tjoelker, R. L. (2016). JPL Ultrastable Trapped Ion Atomic Frequency Standards. *IEEE Transactions on Ultrasonics Ferroelectrics and Frequency Control*, *63*(7), 1013–1021. https://doi.org/10.1109/tuffc.2016.2572701

[21] Enzer, D. G., Diener, W. A., Murphy, D. W., Rao, S. R., & Tjoelker, R. L. (2016). Drifts and environmental disturbances in atomic clock subsystems: quantifying local oscillator, control loop, and ion resonance interactions. *IEEE Transactions on Ultrasonics Ferroelectrics and Frequency Control*, *64*(3), 623–633. https://doi.org/10.1109/tuffc.2016.2636088

[22] Georgakopoulos, D., & Quigg, S. (2017). Precision measurement system for the calibration of PhAsor measurement units. *IEEE Transactions on Instrumentation and Measurement*, *66*(6), 1441–1445. https://doi.org/10.1109/tim.2017.2653518

[23] Zhao, X., Laverty, D. M., McKernan, A., Morrow, D. J., McLaughlin, K., & Sezer, S. (2017). GPS-Disciplined Analog-to-Digital Converter for Phasor measurement applications. *IEEE Transactions on Instrumentation and Measurement*, *66*(9), 2349–2357. https://doi.org/10.1109/tim.2017.2700158

[24] Pulido, V. A., Cabrera-Almeida, F., Quintana-Morales, P., & Mendieta-Otero, E. (2023). Novel phase detector measurement procedure using Quasi-Synchronized RF generator. *IEEE Transactions on Instrumentation and Measurement*, *72*, 1–9. https://doi.org/10.1109/tim.2023.3330210

Baoqiang Du received the Ph.D. degree from Xidian University, Xi'an, China, in 2011. He is a full-time Secondary Professor with the College of Information Science and Engineering, Hunan Normal University, Changsha, China. For over 20 years, he has been actively researching BDS time and frequency measurement for positioning and navigation applications.

Zilin Liu is currently pursuing the Master of Engineering degree in communication engineering with the College of Information Science and Engineering, Hunan Normal University, Changsha, China. He mainly focuses on the research of BDS time and frequency information measurement for applications of satellite navigation and positioning.

Xiang Wang is currently pursuing the Master of Engineering degree in communication engineering with the College of Information Science and Engineering, Hunan Normal University, Changsha, China. He mainly focuses on the research of BDS time and frequency information measurement for applications of satellite navigation and positioning.